# Resistive Wall Mode Instability at Intermediate Plasma Rotation

J. W. Berkery,[1] S. A. Sabbagh,[1] R. Betti,[2] B. Hu,[2] R. E. Bell,[3] S. P. Gerhardt,[3] J. Manickam,[3] and K. Tritz[4]

[1]*Department of Applied Physics and Applied Mathematics, Columbia University, New York, New York 10027, USA*
[2]*Laboratory for Laser Energetics, University of Rochester, Rochester, New York 14623, USA*
[3]*Princeton Plasma Physics Laboratory, Princeton University, Princeton, New Jersey 08543, USA*
[4]*Department of Physics and Astronomy, The Johns Hopkins University, Baltimore, Maryland 21218, USA*

Experimental observation of resistive wall mode (RWM) instability in the National Spherical Torus Experiment (NSTX) at plasma rotation levels intermediate to the ion precession drift and ion bounce frequencies suggests that low critical rotation threshold models are insufficient. Kinetic modifications to the ideal stability criterion yield a more complex relationship between plasma rotation and RWM stability. Good agreement is found between an experimental RWM instability at intermediate plasma rotation and the RWM marginal point calculated with kinetic effects included, by the MISK code. By self-similarly scaling the experimental plasma rotation profile and the collisionality in the calculation, resonances of the mode with the precession drift and bounce frequencies are explored. Experimentally, RWMs go unstable when the plasma rotation is between the stabilizing precession drift and bounce resonances.

Stable operation of future fusion reactors requires eliminating the deleterious effects of magnetohydrodynamic (MHD) modes that limit plasma beta. The ideal MHD kink ballooning mode can be stabilized by the presence of a conducting wall, but this leads to an equally disruptive, though more slowly growing, resistive wall mode (RWM) at plasma beta above the no-wall stability limit. The physics of RWM passive stabilization at high $\beta$ is a key outstanding question for operation of ITER [1].

Theoretically, the RWM is thought to be stabilized by a combination of toroidal plasma rotation, $\omega_\phi$, and energy dissipation mechanisms [2]. Classic models [3] predicted a "critical" rotation sufficient to stabilize the mode, which was characterized by a fraction of the Alfvén frequency at the $q = 2$ surface (typically $\omega_\phi/\omega_A \approx 1\%$) [4]. Recent experiments in the National Spherical Torus Experiment (NSTX) using nonresonant $n = 3$ magnetic braking created passively stable plasmas with $\beta_N > \beta_N^{\text{no-wall}}$ that have $(\omega_\phi/\omega_A)_{q=2} = 0$, challenging this notion. Even a model that uses a critical $\omega_\phi$ profile [5,6] may not be sufficiently broad to explain all experimental results. Balanced neutral beam injection experiments in DIII-D [7] are able to reach low rotation without destabilizing the RWM. In NSTX, however, the RWM can go unstable with a wide range of rotation profiles with $(\omega_\phi/\omega_A)_{q=2} \approx 2\%$–5% [6,8] (Fig. 1). A theoretical model broad enough in scope to explain these results is needed.

In the present work, the theory of kinetic stabilization of the resistive wall mode [1] is directly compared with experimental results from NSTX. This kinetic theory was previously used to assess the stability of ITER [1], where a significant stabilizing effect was predicted. Initial comparison of the theory to DIII-D experimental results [8] resulted in poor agreement. Here it is shown that the kinetic

theory prediction and NSTX experimental observation of marginal stability at intermediate plasma rotation are correlated. The effect of scaling plasma toroidal rotation and collisionality is explored in the theory. It is observed that RWM stability has an intricate dependence on plasma rotation due to resonances with the bounce and precession drift frequencies.

The energy principle including kinetic effects is [1]:

$$(\gamma - i\omega_r)\tau_w = -(\delta W_\infty + \delta W_K)/(\delta W_b + \delta W_K), \quad (1)$$

where $\gamma$ and $\omega_r$ are the RWM growth rate and real frequency, $\tau_w$ is the decay time of current in nearby conducting structures, $\delta W_\infty$ is the fluid no-wall potential energy, $\delta W_b$ is the fluid with-wall potential energy, and $\delta W_K$ is the kinetic contribution, which is complex.

The PEST code [9] is used to calculate the fluid $\delta W$ terms using a marginally stable eigenfunction. Cases are examined which are above the ideal no-wall limit, $-\delta W_\infty/\delta W_b > 0$, and would be unstable without kinetic effects. The Modification to Ideal Stability by Kinetic effects (MISK) code [1], which uses a "perturbative" ap-
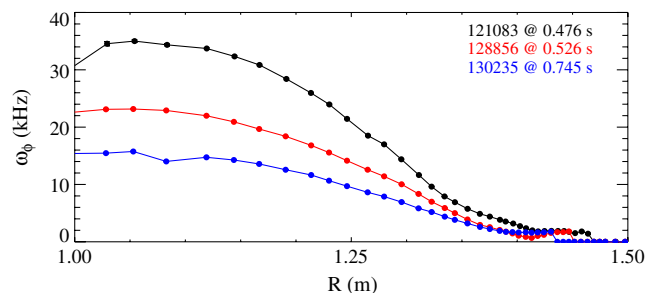


FIG. 1 (color online).  Three measured carbon ion toroidal rotation frequency profiles at RWM marginal stability.

proach, is used to calculate $\delta W_K$. This approach assumes that kinetic effects do not change the eigenfunction, and that the mode growth rate and frequency are small, so their nonlinear inclusion [10] is unimportant [$\gamma$ and $\omega_r$ appear on both sides of Eq. (1), as seen in Eq. (2) below].

The calculation of $\delta W_K$ involves an integration over $\hat{\varepsilon}$ (energy normalized by the ion temperature) of a frequency resonance term [1]. For trapped ions

$$\delta W_K \sim \int_0^\infty \left[ \frac{\omega_{*N} + (\hat{\varepsilon} - \frac{3}{2})\omega_{*T} + \omega_E - \omega_r - i\gamma}{\langle\omega_D\rangle + l\omega_b - i\nu_{\text{eff}} + \omega_E - \omega_r - i\gamma} \right] \hat{\varepsilon}^{5/2} e^{-\hat{\varepsilon}} d\hat{\varepsilon}. \tag{2}$$

Here, the ion diamagnetic frequency $\omega_{*i} = \omega_{*N} + \omega_{*T}$, is the sum of its density and temperature gradient parts, $\omega_E$ is the $E \times B$ frequency, $\langle\omega_D\rangle$ is the bounce-averaged precession drift frequency, $l\omega_b$ is the harmonic times the bounce frequency, and $\nu_{\text{eff}}$ is the collision frequency. The plasma rotation, $\omega_\phi$, enters through $\omega_E = \omega_\phi - \omega_{*i}$, from an ion radial force balance (omitting poloidal rotation, which is negligibly small). The full $\delta W_K$ expression also includes dependence on the RWM eigenfunction [1].

In this theory, the wave-particle resonances $\omega_E \approx -\langle\omega_D\rangle$ and $\omega_E \approx \omega_b$ minimize the denominator of Eq. (2), leading to large $\delta W_K$ and therefore stabilization. These frequencies are shown for NSTX shot 121083 at the marginal time of 0.475 s in Fig. 2(a), as profiles of normalized poloidal flux $\Psi$. Since $\langle\omega_D\rangle^{-1}\hat{\varepsilon}^{5/2}e^{-\hat{\varepsilon}}$ is maximized at $\hat{\varepsilon} = \frac{3}{2}$ and $\omega_b^{-1}\hat{\varepsilon}^{5/2}e^{-\hat{\varepsilon}}$ at $\hat{\varepsilon} = 2$, profiles of $\langle\omega_D\rangle$ and $\omega_b$ at these energies (and zero pitch angle) are shown.
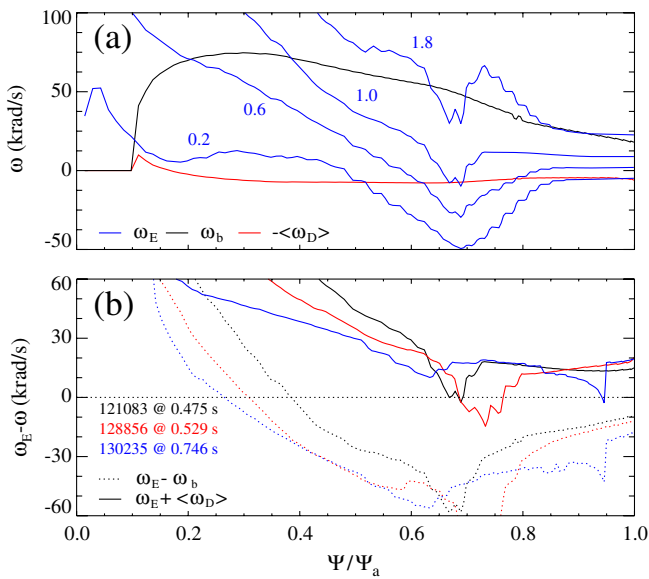


In Fig. 2(a), the $\omega_E$ profile labeled "1.0" is the experimental profile, using $\omega_\phi = \omega_\phi^{\text{exp}}$ from Fig. 1. Note that it lies between $\langle\omega_D\rangle$ and $\omega_b$ for $\Psi/\Psi_a > 0.5$ so that the denominator of Eq. (2) is not minimized, and $\omega_E$ also has a relatively low magnitude, so that the numerator is reduced, leading to small $\delta W_K$ and reduced kinetic stability. The $\omega_E$ profile with rotation profile scaled self-similarly so that $\omega_\phi/\omega_\phi^{\text{exp}} = 1.8$ roughly resonates with the $l = -1$ bounce harmonic, and $\omega_\phi/\omega_\phi^{\text{exp}} = 0.6$ with $\langle\omega_D\rangle$. At low rotation, 0.2, $\omega_E$ is off resonance again, and negative, leading to a large denominator and reduced numerator, reducing kinetic stabilization. Figure 2(b) is a resonance diagram showing that although the three shots in Fig. 1 have very different $\omega_\phi$ profiles at RWM instability, each shot's $\omega_E$ is in-between the stabilizing $\langle\omega_D\rangle$ and $\omega_b$ resonances (resonance occurs if the profile equals zero).

Figure 3 shows the contributions to the real part of $\delta W_K$ vs normalized $\Psi$ for the same NSTX equilibrium as Fig. 2(a), as calculated by MISK, including the effects of trapped ions, trapped electrons, circulating ions, and separately treated Alfvén layers. The equilibrium calculated by EFIT [11] is constrained by motional Stark effect measured magnetic field pitch angle data. The flat areas are rational surface layers where $\delta W_K$ is calculated analytically through inertial enhancement by shear Alfvén damping [12], which appears as higher order terms in the inverse aspect ratio and includes sideband effects [1]. The applied interval around rational $q$ values of $\Delta q = 0.2$ is the smallest that consistently eliminates issues with the numerical calculation. The analytical contributions are then shown averaged over the width of the layer.

A large portion of the kinetic stabilization ($\sim$60% of $\delta W_K$ for trapped ions) comes from the region $q > 2$ where $\omega_E$ is small, and the RWM eigenfunction is large. The circulating ion contribution is small because there is no $l = 0$ harmonic (see Ref. [10]), while the electron contribution is small because $\omega_b$ and $\nu_{\text{eff}}$ both scale as $m^{-(1/2)}$, and so are large in the denominator of Eq. (2) for electrons.

The fluid and kinetic $\delta W$ terms were calculated for several time points of NSTX shot 130235 leading up to the observed time of instability. At each time point, PEST is used to calculate the fluid $\delta W$ terms and then the PEST

FIG. 2 (color online). (a) Frequency profiles for NSTX shot 121083 @ 0.475 s. The four $\omega_E$ profiles shown are calculated with $\omega_\phi/\omega_\phi^{\text{exp}} = 0.2, 0.6, 1.0,$ and 1.8. (b) Profiles of $\omega_E - \omega_b$ and $\omega_E + \langle\omega_D\rangle$ vs $\Psi/\Psi_a$ for the three equilibria of Fig. 1.
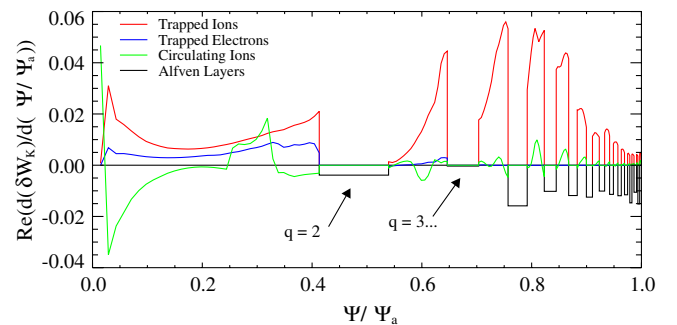


FIG. 3 (color online). Profiles of the components of $\text{Re}(\delta W_K)$ for NSTX shot 121083 @ 0.475 s.
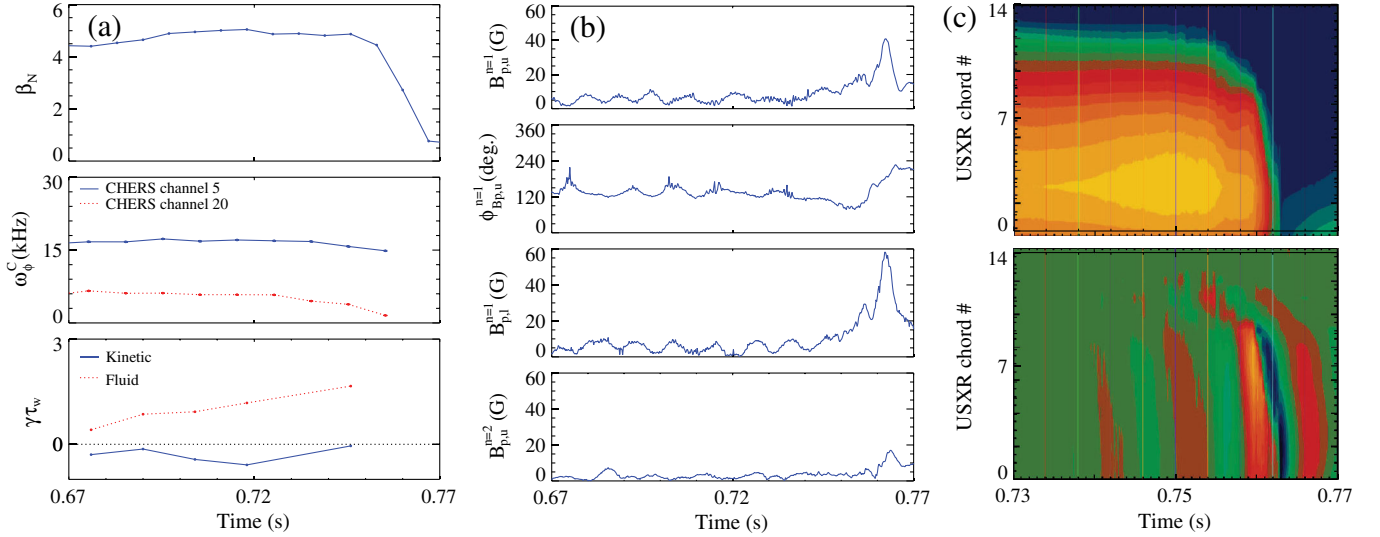
FIG. 4 (color online).   Time traces for NSTX shot 130235: (a) $\beta_N$; measured $\omega_\phi$ for carbon ions near the axis (ch. 5) and near the $q = 2$ surface (ch. 20); PEST calculated fluid and MISK calculated kinetic RWM $\gamma\tau_w$. (b) Mode amplitude of $n = 1$ poloidal field perturbation from the upper RWM sensor array; $B_p^{n=1}$ upper sensor phase and; $B_p^{n=1}$ lower; and $B_p^{n=2}$ upper amplitudes. (c) Ultrasoft x-ray contours of amplitude (top) and phase (bottom), from core (0) to edge (14).

results and the experimental density, temperature, and rotation profiles are used to calculate $\delta W_K$ with MISK. In Fig. 4(a), as the time approaches 0.746 s, the calculated kinetic growth rate comes very close to marginal stability ($\gamma\tau_w = 0$), consistent with the observation of an unstable RWM soon after. The mode is identified as a RWM by a slow drift of the $n = 1$ mode in the co-NBI direction, indicated by the $B_p$ sensor phase, coincident with the detection of a growing signal on low frequency ($f < 2.5$ kHz) poloidal magnetic sensors [Fig. 4(b)], the global nature of the mode, extending from edge to core in USXR channels with no clear phase inversion [Fig. 4(c)], and the lack of rapidly rotating ($f \sim \omega_\phi/2\pi$) MHD mode spectrum activity and local flattening of the rotation profile that would indicate a tearing mode (not shown).

A stability condition can be written by separating out the normalized growth rate from Eq. (1), and rewriting:

$$(\mathrm{Re}(\delta W_K) - a)^2 + (\mathrm{Im}(\delta W_K))^2 = r^2, \qquad (3)$$

$$r = (\delta W_b - \delta W_\infty)/(2(1 + \gamma\tau_w)), \qquad (4)$$

$$a = -\frac{1}{2}(\delta W_b + \delta W_\infty) - \frac{1}{2}(\delta W_b - \delta W_\infty)\frac{\gamma\tau_w}{1 + \gamma\tau_w}. \qquad (5)$$

On a plot of $\mathrm{Im}(\delta W_K)$ vs $\mathrm{Re}(\delta W_K)$, contours of constant $\gamma\tau_w$ form circles with offset $a$ and radius $r$. The plasma is stable if $\mathrm{Re}(\delta W_K)$ and $\mathrm{Im}(\delta W_K)$ lie outside of a circle centered at $(-\frac{1}{2}(\delta W_b + \delta W_\infty), 0)$ with radius $\frac{1}{2}(\delta W_b - \delta W_\infty)$. If $\mathrm{Re}(\delta W_K) > -\frac{1}{2}(\delta W_b + \delta W_\infty)$, then increasing $\mathrm{Re}(\delta W_K)$ decreases the growth rate. Increasing $|\mathrm{Im}(\delta W_K)|$ always decreases the growth rate. Figure 5(a) is an example of such a stability diagram with unstable region ($\gamma\tau_w > 0$) shown shaded in yellow. The experimental point, labeled "1.0", is close to marginal stability.
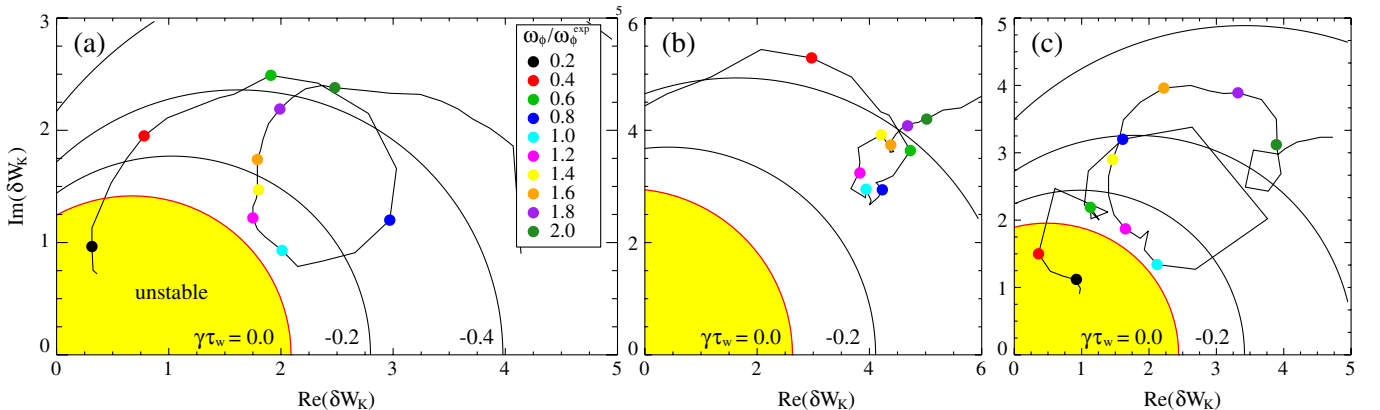


FIG. 5 (color online).   RWM stability diagrams for NSTX: (a) 121083 @ 0.475 s, (b) 128856 @ 0.529 s, and (c) 130235 @ 0.746 s.

To theoretically test the effect of rotation on stability, the experimental rotation profile, $\omega_\phi^{\mathrm{exp}}$, is then varied self-similarly by a factor of 0 to 4. The results are shown in the diagram, with representative values of $\omega_\phi/\omega_\phi^{\mathrm{exp}}$ labeled by markers (not all points are labeled). For very low rotation, the plasma is predicted to be unstable. This is consistent with the traditional view of a critical rotation value, below which the plasma is RWM unstable. For $\omega_\phi/\omega_\phi^{\mathrm{exp}}$ from 0 to 0.6 stability increases as the real and imaginary trapped ion components increase. This is due to the resonance with $\langle\omega_D\rangle$, which is a fraction of $\omega_E$ [Fig. 2(a)]. Near the experimental rotation value $\omega_E$ is between resonances, so there are local minima in $\mathrm{Re}(\delta W_K)$ and $\mathrm{Im}(\delta W_K)$, leading to the turn in Fig. 5 back towards instability. Similar local minimum behavior was seen in calculations of $\delta W_K$ vs $\omega_\phi$ with the MISHKA code for JET [13]. Finally, for $\omega_\phi/\omega_\phi^{\mathrm{exp}} > 1$, the resonance with $\omega_b$ becomes important and $\mathrm{Im}(\delta W_K)$ goes towards zero while $\mathrm{Re}(\delta W_K)$ approaches a large constant value, continuing the trend in Fig. 5(a) out to a very stable point.

Figures 5(b) and 5(c) are stability diagrams for the other two equilibria from Fig. 1. In each case the kinetic stabilizing effects are reduced when $\omega_E$ is off resonance, but in the case of Fig. 5(b), the stability reduction is not enough to quantitatively reach marginal stability. Such cases may indicate an unknown shortcoming or sensitivity of the code. One of the largest sensitivities is the width of the Alfvén layers, $\Delta q$. A change of $\Delta q$ by $\pm0.05$ results, roughly, in a change of $\gamma\tau_w$ by $\pm0.1$.

In addition to the effect of rotation, it is interesting to look at the effect of collisionality on stability in the kinetic model. In simple models, collisions increase stability because they increase the dissipation of the mode energy [6]. A realistic test of the effect of collisionality in the kinetic model is to change $\nu_{\mathrm{eff}}$ in the calculation by multipling density by a constant while dividing temperature by the same constant. This keeps $\beta$ constant while changing *all* of the plasma frequencies in Eq. (2). Figure 6 shows contours of $\gamma\tau_w$ on a plot of collisionality scaled in this manner vs scaled rotation. The actual experimental condition, at location (1,1), is marked.

At low rotation this diagram appears to show a classic critical rotation value below which the plasma is unstable. A scalar $(\omega_\phi/\omega_A)_{q=2}$ is included on the plot's upper axis for comparison purposes; the value of $\approx1\%$ is roughly consistent with previously quoted critical rotation values [4]. However, there is also a band of marginal stability at intermediate rotation (which occurs when the loop in Fig. 5(a) comes close to the unstable regime) where the plasma actually goes unstable in the experiment (at $(\omega_\phi/\omega_A)_{q=2} \approx 4\%$ for NSTX [4]). This behavior results
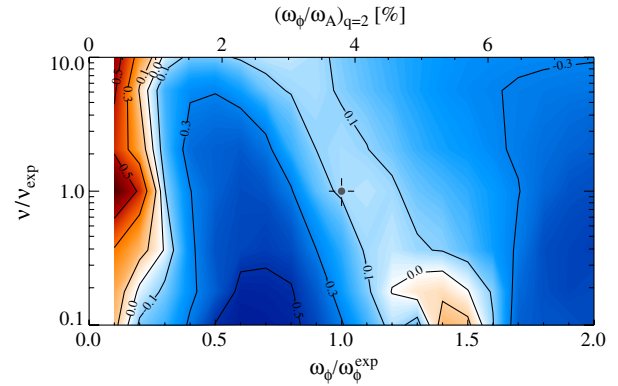


FIG. 6 (color online). Contours of $\gamma\tau_w$ for NSTX 121083 at 0.475 s. Blue ($<0$) is stable and red ($>0$) unstable.

when the $\omega_E$ is roughly in between $\langle\omega_D\rangle$ and $\omega_b$ resonances in the outer surfaces where kinetic stabilization mainly occurs [compare Figs. 2(a), 5(a), and 6]. Note that changing $\nu/\nu^{\mathrm{exp}}$ over 2 orders of magnitude has less impact than changing $\omega_\phi/\omega_\phi^{\mathrm{exp}}$ from 0 to 2, but does shift the rotation level that is marginally stable.

Future analysis with the MISK code for NSTX will include the expected stabilizing effects of energetic particles. A strong energetic particle component of kinetic stabilization could help explain previous discrepancies between kinetic theory and experiment in DIII-D [8], and possibly the recently observed energetic particle mode triggered RWMs as well [14].

[1]  B. Hu *et al.*, Phys. Plasmas **12**, 057301 (2005).
[2]  A. Bondeson and D. Ward, Phys. Rev. Lett. **72**, 2709 (1994).
[3]  R. Fitzpatrick and A. Aydemir, Nucl. Fusion **36**, 11 (1996).
[4]  H. Reimerdes *et al.*, Phys. Plasmas **13**, 056107 (2006).
[5]  S. Sabbagh *et al.*, Nucl. Fusion **46**, 635 (2006).
[6]  A. Sontag *et al.*, Nucl. Fusion **47**, 1005 (2007).
[7]  H. Reimerdes *et al.*, Phys. Rev. Lett. **98**, 055001 (2007).
[8]  H. Reimerdes *et al.*, Plasma Phys. Controlled Fusion **49**, B349 (2007).
[9]  R. Grimm *et al.*, *Methods in Computational Physics* (Academic Press, New York, 1976), Vol. 16, p. 253.
[10]  Y. Liu *et al.*, Phys. Plasmas **15**, 112503 (2008).
[11]  S. Sabbagh *et al.*, Nucl. Fusion **41**, 1601 (2001).
[12]  L. Zheng *et al.*, Phys. Rev. Lett. **95**, 255003 (2005).
[13]  I. Chapman *et al.*, Plasma Phys. Controlled Fusion **51**, 055015 (2009).
[14]  G. Matsunaga *et al.*, Phys. Rev. Lett. **103**, 045001 (2009).